Potential energy surfaces for Ar–OH ($X\,^2\Pi$) obtained by fitting to high-resolution spectroscopy

Marie-Lise Dubernet and Jeremy M. Hutson

Citation: The Journal of Chemical Physics **99**, 7477 (1993); doi: 10.1063/1.465729
View online: http://dx.doi.org/10.1063/1.465729
View Table of Contents: http://aip.scitation.org/toc/jcp/99/10
Published by the American Institute of Physics

Potential energy surfaces for Ar–OH ($X\,^2\Pi$) obtained by fitting to high-resolution spectroscopy

Marie-Lise Dubernet and Jeremy M. Hutson
Department of Chemistry, University of Durham, South Road, Durham DH1 3LE, England

(Received 16 June 1993; accepted 6 August 1993)

Empirical potential energy surfaces for Ar interacting with OH ($X\,^2\Pi$) are obtained by fitting to experimental results from microwave and stimulated-emission pumping (SEP) spectra of the Ar–OH complex. The sum V_Π and difference V_2 of the potentials for A' and A'' symmetry are determined. The sum potential is 126 cm^{-1} deep, which is about 24 cm^{-1} deeper than the *ab initio* CEPA potential of Degli Esposti and Werner [J. Chem. Phys. **93**, 3351 (1990)]. The equilibrium geometry is near-linear, Ar—H–O, with a barrier to internal rotation of 44 cm^{-1}. The potential satisfactorily reproduces all the parameters obtained from the SEP experiments, but not the parity doubling obtained from the microwave spectrum.

I. INTRODUCTION

There has been a great deal of experimental and theoretical interest in the open-shell complex Ar–OH.[1] Electronic transitions correlating with the $A\,^2\Sigma \leftarrow X\,^2\Pi_{3/2}$ band system of OH and OD have been observed by Fawzy and Heaven[2,3] and by Lester and co-workers.[4–8] These experiments allowed the vibrational structure of Ar–OH in the $A\,^2\Sigma$ state to be mapped out, and have been used by Bowman and co-workers[9,10] to determine potential energy surfaces for Ar–OH ($A\,^2\Sigma$). More recently, Schleipen *et al.*[11] and Chang *et al.*[12] have observed the absorption spectra under higher resolution, and Lester *et al.*[13] have extended the measurements to additional bands and have refined the intermolecular potential for the A state. In addition, Berry *et al.*[14,15] have observed stimulated-emission pumping (SEP) spectra that map out the vibrational levels of the electronic ground state, $X\,^2\Pi$, and provide some rotational information, and Ohshima, Iida, and Endo[16] have measured microwave spectra of the ground vibronic state.

In parallel with the experimental work, there has been a substantial amount of theoretical work. Degli Esposti and Werner[17] have performed high-quality *ab initio* calculations in the correlated electron pair approximation (CEPA), and have obtained potential energy surfaces for Ar–OH in both the $X\,^2\Pi$ and $A\,^2\Sigma$ states. Chakravarty and Clary[18] have used these to simulate both the absorption spectra and the SEP spectra. Dubernet, Flower, and Hutson[19] have developed the theory needed to understand the energy levels of open-shell complexes, and have considered the various possible angular momentum coupling schemes. Green and Lester[20] have developed a perturbative scheme for the parity doubling in the $P=\frac{1}{2}$ excited bending state of the complex, and this has been extended to handle the ($P=\frac{3}{2}$) ground state by Dubernet, Tuckey, and Hutson.[21]

One of the major reasons for studying the spectra of van der Waals complexes is that they provide a sensitive probe of the intermolecular potential.[22] Ar–OH is the first system to provide a realistic opportunity of obtaining detailed experimental information on an intermolecular potential involving a molecule in a $^2\Pi$ state. The *ab initio* calculations of Degli Esposti and Werner[17] provide a first estimate of the potential, but it is known that CEPA calculations tend to underestimate dispersion forces substantially: Since the attractive forces in Ar–OH ($X\,^2\Pi$) are dominated by dispersion, the *ab initio* well depth is expected to be considerably too shallow. This has been confirmed by Chakravarty and Clary,[18] who showed that the van der Waals stretching frequencies calculated from the CEPA potential are significantly lower than those observed experimentally.

The aim of the present paper is to determine the intermolecular potential of Ar–OH ($X\,^2\Pi$) as accurately as possible from the spectroscopic measurements. The structure of the paper is as follows. Section II describes the computational methods used to calculate spectroscopic parameters from a trial potential energy surface. Section III describes the parametrization of the potential used in the least-squares fits. Section IV provides a description of the methods used to fit the experimental spectroscopic data and gives the resulting parametrized potential. The predictions of the spectroscopic observables, based on the fitted potential, are listed in Sec. V.

II. COMPUTATIONAL METHOD

The Ar–OH complex is described in the usual Jacobi coordinate system used for atom–diatom complexes. The monomer bond vector, from the O atom to the H atom, is denoted **r** and has length r. The intermolecular vector, from the OH center of mass to the Ar atom, is denoted **R** and has length R. The angle between **R** and **r** is θ: θ is 0 at the linear Ar—H–O geometry and 180° at the linear Ar—O–H geometry. All the spectra considered in the present work relate to the ground vibrational state of the OH monomer; since the OH vibration is of much higher frequency than the van der Waals modes, the r coordinate is averaged over, and the potentials obtained are effective potentials for OH in its $v=0$ state.

The quantum numbers appropriate for describing the energy levels of Ar–OH ($X\,^2\Pi$) have been discussed by Dubernet, Flower, and Hutson.[19] Lower-case letters are used for quantum numbers that refer to the OH monomer,

and capital letters are used for quantum numbers that refer to the complex as a whole. The energy levels are best described in a body-fixed coupling scheme. The total angular momentum of the OH monomer j is approximately conserved in the complex, but the anisotropy of the intermolecular potential causes it to become coupled to the intermolecular axis **R** with projection P. The projection of j onto the *monomer* axis **r** is ω, and the *relative sign* of P and ω is crucial in determining the energy levels, because it determines whether the wave function is concentrated around the Ar—O–H geometry or around the Ar—H–O geometry. To simplify the notation in the present paper, P is given as positive when P and ω have the same sign, and negative when they have different sign.

Even though the real wave functions are most compactly described by body-fixed quantum numbers, we have chosen to carry out the *exact* calculations described below in a space-fixed basis set, because the matrix elements of the Hamiltonian are simpler. Provided all possible L values are included in the calculation for a given J, the results of exact calculations in space- and body-fixed basis sets should be identical.

In spectroscopic applications, where information on intermolecular potentials is to be inferred from small differences between observed and calculated quantities, it is very important for the monomer energy levels to be represented accurately. In the present work, the OH monomer energy levels and wave functions are obtained by diagonalizing the effective Hamiltonian of Brown *et al.*,[23] using a basis set of Hund's case (a) functions, with molecular parameters taken from Coxon.[24] The effective Hamiltonian is expressed as

$$\mathscr{H}_{\rm eff}=H_{\rm so}+H_{\rm rot}+H_{\rm cd}+H_{\rm sr}+H_{\rm ld}+H_{\rm cdld}, \tag{1}$$

where $H_{\rm so}$ represents the spin–orbit coupling, $H_{\rm rot}$ and $H_{\rm cd}$ represent the rotational kinetic energy and centrifugal distortion, $H_{\rm sr}$ represents the spin–rotation coupling, and $H_{\rm ld}$ and $H_{\rm cdld}$ represent the λ doubling and its centrifugal distortion. $\mathscr{H}_{\rm eff}$ operates only within the spin and rotational levels of a given vibronic state, and includes the effects of any perturbing states through the effective parameters. The Hamiltonian matrix is constructed in a basis set of symmetrized functions with definite parity $p=\epsilon(-1)^{j-s}$,

$$|\lambda s\sigma,jm_j\omega p\rangle=(2)^{-1/2}[\,|jm_j\omega\rangle\,|\lambda s\sigma\rangle +\epsilon|jm_j-\omega\rangle\,|-\lambda s-\sigma\rangle], \tag{2}$$

where $|\lambda s\sigma\rangle$ is an adiabatic electronic wave function and $|jm_j\omega\rangle$ is a normalized symmetric top rotational function

$$\langle\theta,\phi\,|jm_j\omega\rangle=\left(\frac{2j+1}{4\pi}\right)^{1/2}\mathscr{D}^{j*}_{m_j\omega}(\phi,\theta,0). \tag{3}$$

Since the effective Hamiltonian is diagonal in j, m_j, and p, a simple 2×2 diagonalization gives the monomer eigenvalues, $E^{\rm mon}_{jp\tau}$, and eigenvectors,

$$|jm_jp\tau\rangle=\sum_{\omega=1/2,3/2}a^{jp\tau}_{\omega}|\lambda s\sigma,jm_j\omega p\rangle, \tag{4}$$

where $\tau=1$ labels the states that are principally of $\omega=\frac{3}{2}$ character, and $\tau=2$ labels the states that are principally of $\omega=\frac{1}{2}$ character.

The total Hamiltonian of the complex is

$$-\frac{\hbar^2}{2\mu}R^{-1}\left(\frac{\partial^2}{\partial R^2}\right)R+\mathscr{H}_{\rm eff}+\frac{\hbar^2\hat{L}^2}{2\mu R^2}+V(R,\theta). \tag{5}$$

This is exactly the same as for a closed-shell atom–diatom complex,[25] except that the monomer Hamiltonian is more complicated. The space-fixed angular basis functions for the complex are formed by coupling the monomer functions with spherical harmonics for the end-over-end rotation to form eigenfunctions of the total angular momentum operator $\hat{J}^2$,

$$\mathscr{Y}^{JM}_{jp\tau L}=\sum_{m_jm_L}\langle jm_jLm_L|JM\rangle\,|jm_jp\tau\rangle\,|Lm_L\rangle. \tag{6}$$

The quantum numbers j and J are of course half-integer for Ar–OH. The overall parity of the basis functions is $p'=(-1)^Lp$. The total wave function of the complex is then expanded in terms of these basis functions,

$$\Psi=R^{-1}\sum_{jp\tau L}\mathscr{Y}^{JM}_{jp\tau L}\chi^J_{jp\tau L}(R). \tag{7}$$

A set of coupled equations is obtained by substituting the expansion of Eq. (7) into the full Schrödinger equation, multiplying from the left by the complex conjugate of each of the angular basis functions (6) in turn, and integrating over all angular variables. The coupled equations take the form

$$\left[-\frac{\hbar^2}{2\mu}\frac{d^2}{dR^2}+(jp\tau LJ|\,V\,|jp\tau LJ)+\frac{\hbar^2L(L+1)}{2\mu R^2} +E^{\rm mon}_{jp\tau}-E\right]\chi^J_{jp\tau L}(R) =-\sum_{j'p'\tau'L'}{}'(jp\tau LJ|\,V\,|j'p'\tau'L'J)\chi^J_{j'p'\tau'L'}(R), \tag{8}$$

where $(jp\tau LJ|\,V\,|j'p'\tau'L'J)$ are R-dependent matrix elements of the interaction potential between the angular basis functions of Eq. (6), and may be expressed in terms of the matrix elements between the primitive functions of Eq. (2) given by Klar[26] and Alexander.[27] The interaction of an atom with a $^2\Pi$ diatom is described by two intermolecular potential surfaces, depending on whether the unpaired π electron is parallel (A') or perpendicular (A'') to the molecular plane. The sum and difference of these two potentials may be expanded in terms of renormalized spherical harmonics $C^m_l(\theta,0)$,

$$V_\Pi(R,\theta)=\tfrac{1}{2}[V_{A''}(R,\theta)+V_{A'}(R,\theta)] =\sum_l V_{l0}(R)C^0_l(\theta,0), \tag{9}$$

$$V_2(R,\theta)=\tfrac{1}{2}[V_{A''}(R,\theta)-V_{A'}(R,\theta)] =\sum_l V_{l2}(R)C^2_l(\theta,0), \tag{10}$$

where $C_l^0(\theta,\phi)=P_l(\cos\theta)$. $V_\Pi(R,\theta)$ contributes matrix elements diagonal in λ and σ (and hence diagonal in ω), while $V_2(R,\theta)$ contributes matrix elements diagonal in σ but with $\Delta\lambda=\pm2$, which couple the $\omega=\pm\frac{1}{2}$ and $\omega=\pm\frac{3}{2}$ manifolds.

In the present work, the coupled equations (8) are solved by the log-derivative shooting method of Johnson,[28] using the BOUND program.[29,25] The log derivative of the wave function is propagated outwards from a boundary point at short range ($R_{\min}$) and inwards from a boundary point at long range ($R_{\max}$) to a matching point (R_{mid}) in the classically allowed region. If E is an eigenvalue of the Hamiltonian, the determinant of the difference between the two log-derivative matrices at R_{mid} is zero. Eigenvalues are located by searching for zeroes of the matching determinant, using bisection followed by the secant method.

The basis set used is the present work included all channels with $j\leqslant 9/2$.

III. PARAMETRIZATION OF THE INTERMOLECULAR POTENTIAL

The dynamical calculations require potential coefficients $V_{lm}(R)$ as defined in Eqs. (9) and (10). However, as described below, we found that parametrizing the coefficients $V_{lm}(R)$ directly did not give well-behaved fits to the experimental data. Instead, as in the well-understood rare gas–hydrogen halide systems,[22] the parameters defining V_Π (ϵ^Π, R_m^Π, and β^Π) are expanded in Legendre polynomials

$$\epsilon^\Pi(\theta)=\sum_l \epsilon_{l0}^\Pi P_l(\cos\theta), \tag{11}$$

$$R_m^\Pi(\theta)=\sum_l [R_m^\Pi]_{l0} P_l(\cos\theta), \tag{12}$$

$$\beta^\Pi(\theta)=\sum_l \beta_{l0}^\Pi P_l(\cos\theta). \tag{13}$$

At each value of θ, the radial potential is

$$V_\Pi(R,\theta)=A^\Pi(\theta)\exp[-\beta^\Pi(\theta)R]+V_\Pi^{\mathrm{ind}}(R,\theta) - \sum_{n=6}^{8} C_n^\Pi(\theta) D_n(R) R^{-n}. \tag{14}$$

The induction and dispersion terms up to order R^{-7} are constrained to theoretical values and the coefficients $C_8^\Pi(\theta)$ and $A^\Pi(\theta)$ are calculated (for each value of θ) to reproduce the required $\epsilon^\Pi(\theta)$ and $R_m^\Pi(\theta)$ as described in the Appendix of Ref. 30. The difference potential $V_2(R,\theta)$ is expanded separately, as described below.

The leading long-range terms in the potential are constrained to follow the theoretically known behavior. For a diatomic molecule in a Π state, such as ground-state OH, the two axes x and y perpendicular to the internuclear axis z are in principal different, so that electrical properties such as the quadrupole moment and polarizability tensors do not have cylindrical symmetry. Unfortunately, the only calculations available for OH electrical properties[17] do not distinguish between the x and y axes, so that in the present work it was necessary to assume cylindrical symmetry. Within this approximation, the leading terms in the long-range potential are (to order R^{-7})

$$V_\Pi^{\mathrm{ind}}(R,\theta)=-\alpha_{\mathrm{Ar}}\mu_{\mathrm{OH}}^2[1+P_2(\cos\theta)]R^{-6} - 6\alpha_{\mathrm{Ar}}\mu_{\mathrm{OH}}\Theta_{\mathrm{OH}}\cos^3\theta R^{-7}, \tag{15}$$

$$C_6^\Pi(\theta)=[C_6]_{00}+[C_6]_{20}P_2(\cos\theta), \tag{16}$$

$$C_7^\Pi(\theta)=[C_7]_{10}P_1(\cos\theta)+[C_7]_{30}P_3(\cos\theta), \tag{17}$$

where

$$[C_6]_{20}=\left(\frac{\alpha_{zz}-\alpha_\perp}{3\bar\alpha}\right)[C_6]_{00}, \tag{18}$$

$$[C_7]_{10}=6\left(\frac{2A_\perp+A_\parallel}{5\bar\alpha}\right)[C_6]_{00}, \tag{19}$$

$$[C_7]_{30}=2\left(\frac{6A_\parallel-8A_\perp}{15\bar\alpha}\right)[C_6]_{00}, \tag{20}$$

$$\alpha_\perp=\tfrac{1}{2}(\alpha_{xx}+\alpha_{yy}), \tag{21}$$

$$\bar\alpha=\tfrac{1}{3}(\alpha_{xx}+\alpha_{yy}+\alpha_{zz}). \tag{22}$$

The notation for molecular properties is that of Buckingham,[31] and the subscripts xx, yy, and zz apply to properties of OH. The OH multipole moments and polarizabilities and the dipole polarizability of Ar used in the present work are summarized in Table I. The isotropic coefficient $[C_6]_{00}$ is taken to be 44.726 $E_h a_0^6$, based on the combining rule described in Ref. 32.

TABLE I. Electrical properties of OH and Ar used in evaluating long-range potentials.

μ_{OH}/ea_0	0.654
$\Theta_{\mathrm{OH}}/ea_0^2$	1.391
$\bar\alpha/a_0^3$	7.82
$(\alpha_{zz}-\alpha_\perp)/a_0^3$	2.4
$A_\parallel/a_0^4$	8.29
$A_\perp/a_0^4$	1.48
$\alpha_{\mathrm{Ar}}/a_0^3$	11.06

In the present work, the dispersion damping functions appearing in Eq. (14) are taken to be the damping functions $D_n(R)$ proposed by Tang and Toennies,[33]

$$D_n(R)=1-\exp(-\beta R)\sum_{m=0}^{n}\frac{(\beta R)^m}{m!}. \tag{23}$$

The quantities actually varied in the least-squares fits are the Legendre components of $\epsilon^\Pi(\theta)$, $R_m^\Pi(\theta)$ and $\beta^\Pi(\theta)$. However, the dynamical calculations still require adiabatic electronic potentials expressed as an expansion in Legendre polynomials (or spherical harmonics) at each R. To obtain these, $V_\Pi(R,\theta)$ is evaluated at 12 Gauss–Legendre quadrature points and the coefficients of the first five Legendre coefficients are projected out using standard quadrature techniques.[34]

The difference potential $V_2(R,\theta)$ is parametrized as

TABLE II. Comparison of observed and calculated spectroscopic properties of Ar–OH for the *ab initio* and fitted potentials. The experimental data come mostly from Ref. 14, apart from $\Delta\nu_{3/2}$ and $B^0_{3/2}$ (Ref. 15). The parity doubling $\Delta\nu_{3/2}$ is not included in the present fit. All quantities are in cm^{-1}.

		Potential A (*ab initio*)		Best fit		
Ar–OH($^2\Pi$,v=0)	Observed	Calc.	Obs.–Calc.	Calc.	Obs.–Calc.	Uncertainty
Ground stretch, n=0						
$E^0_{1/2}-E^0_{3/2}$	9.7	9.49	+0.21	9.695	+0.005	0.20
$E^0_{-1/2}-E^0_{3/2}$	19.2	16.61	+2.58	19.199	+0.001	0.20
$E^0_{-3/2}-E^0_{3/2}$	21.3	17.18	+4.11	21.300	0.000	0.20
$B^0_{3/2}$	0.1025	0.0932	+0.0093	0.1025	0.0000	0.0005
$B^0_{1/2}$	0.105	0.0995	+0.005	0.107	−0.002	0.01
$\Delta\nu_{1/2}(J=3/2)$	0.230	0.575	−0.345	0.2305	−0.0005	0.03
$\Delta\nu_{3/2}(J=3/2)/10^{-5}$	16.86	9.84	+6.96	[7.29]	[+9.57]	
First excited stretch, n=1						
$E^1_{3/2}-E^0_{3/2}$	34.9	26.90	+8.00	34.877	+0.023	0.20
$E^1_{1/2}-E^1_{3/2}$	6.1	6.36	−0.26	6.39	−0.29	1.00
$B^1_{3/2}$	0.099	0.0835	+0.0155	0.0924	+0.0066	0.01
Second excited stretch, n=2						
$E^2_{3/2}-E^0_{3/2}$	60.00	46.00	+14.00	60.56	−0.56	1.00
$E^2_{1/2}-E^2_{3/2}$	4.00	4.066	−0.066	4.088	−0.088	1.00
Third excited stretch, n=3						
$E^3_{3/2}-E^0_{3/2}$	78.00	58.09	+19.91	78.06	+0.06	1.00
$E^3_{1/2}-E^3_{3/2}$	3.00	2.30	+0.70	2.58	+0.420	1.00

$$V_2(R,\theta)=v^{(2)}f(\theta)\exp[-\beta^{(2)}(R-R_c)] - [C_6]_{22}D_6(R)R^{-6}C_2^2(\theta,0), \quad (24)$$

where R_c is a fixed reference distance in the vicinity of $[R^{\Pi}_m]_{00}$. The angular function $f(\theta)$ appearing in the short-range term may either be taken to be the leading spherical harmonic term $C_2^2(\theta,0)$, or may use a more specialized functional form as described below.

Most of the results reported in the present paper were obtained with the approach described above, which we found to give reasonably smooth convergence of the fits and well-determined parameters. However, we also put considerable effort into fitting with alternative approaches in which the individual coefficients $V_{lm}(R)$ were parametrized in a number of different ways. These alternative approaches were helpful because they allowed us to investigate the relationships between potential features and spectroscopic observables. However, they did not in the end give useful fits because of the difficulty of imposing physically sensible constraints on the values of undetermined parameters.

IV. SPECTROSCOPIC DATA AND METHOD OF FIT

The quantum numbers that describe the energy levels of Ar–OH ($X\,^2\Pi$) have been investigated by Dubernet, Flower, and Hutson.[19] The monomer angular momentum j is nearly conserved, and has projection P onto the intermolecular axis. Each monomer j state is split into $2j+1$ components of different P by the potential anisotropy. The ground state of OH ($X\,^2\Pi$) has $j=\frac{3}{2}$ and $\omega=\frac{3}{2}$, and is thus split into four "bending" states: The ground state of the complex has $P=+\frac{3}{2}$, and the first excited state has $P=+\frac{1}{2}$; the other two bending states, $P=-\frac{1}{2}$ and $-\frac{3}{2}$, are relatively closely spaced, and are significantly mixed by Coriolis couplings. In addition, there is a Van der Waals stretching quantum number n. For each vibrational state (labeled by j,ω,P,n), there is a ladder of rotational states with $J\geqslant|P|$. Each rotational level is split into two states of different total parity, designated J^+ and J^-, by couplings involving the V_2 part of the intermolecular potential, Coriolis coupling $B\hat{j}\cdot\hat{J}$ and the monomer rotational decoupling interaction $b\hat{j}_\pm\hat{s}_\pm$.

The experiments that contain the most information on the Ar–OH ($X\,^2\Pi$) interaction potential are the stimulated-emission pumping (SEP) spectra of Berry *et al.*[14,15] The SEP spectra provide vibrational energy spacings between the ground state ($n=0$, $P=+\frac{3}{2}$) and a number of bending- and stretching-excited states, including the $P=+\frac{1}{2}$, $P=-\frac{1}{2}$, and $P=-\frac{3}{2}$ states for the stretching ground state, $n=0$. For $n=1$, 2, and 3, the closely spaced $P=-\frac{1}{2}$ and $P=-\frac{3}{2}$ peaks are not resolved. Some peaks due to transitions to $j=5/2$ levels were also observed, but could not be assigned to specific P values. The SEP spectra are not yet fully rotationally resolved, but Berry *et al.*[14] were nevertheless able to obtain approximate rotational constants for the $n=0$, $P=+\frac{3}{2}$, $n=0$, $P=+\frac{1}{2}$, and $n=1$, $P=+\frac{3}{2}$ levels and a parity splitting (P-type doubling constant) for the $n=0$, $P=+\frac{1}{2}$ level. Schleipen *et al.*[11] and Chang *et al.*[12] have measured the rotational constant of the $n=0$, $P=+\frac{3}{2}$ ground state to greater precision, and have obtained an upper bound for the parity splitting. Finally, Ohshima, Iida, and Endo[16] have measured the microwave spectrum of the $n=0$, $P=+\frac{3}{2}$ state, and have obtained the rotational constant and parity doubling splitting to high precision.

The experimental quantities included in our fits are summarized in Table II, along with the uncertainties used.

In our calculations, rotational constants B_P^n and parity splittings $\Delta\nu_P^n$ are calculated from eigenvalue differences, using the energy expressions

$$E_P^n(J^{\pm}) = E_P^n + B_P^n[J(J+1) - P^2] \pm \tfrac{1}{2}\Delta\nu_P^n, \tag{25}$$

using the four bound states $E_P^n(J=P^{\pm})$ and $E_P^n(J=P+1^{\pm})$. The eigenvalues themselves are obtained from close-coupling calculations as described above.

The ways in which various features of the intermolecular potential influence the spectroscopic observables have been discussed by Dubernet *et al.*[19,21] and by Green and Lester.[20] The coefficients ϵ_{l0}^{Π} principally affect the expectation values $\langle V_{l0}(R)\rangle$, which determine the separation of the different bending (P) states. The parameters for the position of the minimum $[R_m^{\Pi}]_{l0}$ determine the rotational constants for the different states. States of different P sample the angular potential differently: States with $P=+j$ are concentrated around $\theta=0$, while states with $P=-j$ are concentrated around $\theta=180°$; states with intermediate P sample intermediate angles.

As discussed by Green and Lester[20] and Dubernet, Tuckey, and Hutson,[21] $V_2(R,\theta)$ has some effect on the bending energy levels, but principally determines the parity splittings. Perturbation theory gives respectively third- and fifth-order expressions for the parity splittings of the $P=+\frac{1}{2}$ and $P=+\frac{3}{2}$ states,

$$\Delta\nu_{1/2} = C_p\langle V_{22}\rangle(J+\tfrac{1}{2}); \tag{26}$$

$$\Delta\nu_{3/2} = C_q\langle V_{22}\rangle(J-\tfrac{1}{2})(J+\tfrac{1}{2})(J+\tfrac{3}{2}), \tag{27}$$

where the superscripts n have been omitted for clarity; parity doubling has so far been measured only for $n=0$ states. The coefficients C_p and C_q involve the rotational constants of both the monomer and the complex and a function that depends on the spacings of the bending levels in the $\omega=\frac{1}{2}$ and $\frac{3}{2}$ manifolds. The experimental parity splittings should thus provide information on the difference potential.

As mentioned above, bending frequencies have been observed for several different van der Waals stretching quantum numbers n. The stretching frequencies are mainly determined by the depth and shape of the isotropic potential $V_{00}(R)$. However, in addition, the bending frequencies are slightly different in the different stretching states, because they involve different averages over the radial strength functions $V_{l0}(R)$. The R dependence of these functions is controlled mainly by the parameters $[R_m^{\Pi}]_{l0}$ and β_{l0}^{Π}; thus the changes in bending frequencies when the van der Waals stretch is excited provide additional information on $[R_m^{\Pi}]_{10}$ and $[R_m^{\Pi}]_{20}$, β_{10}^{Π} and β_{20}^{Π}.

We began by choosing potential parameters based on the *ab initio* potential of Ref. 17, and obtained the parameters shown in the first column of Table I; this parametrized form of the *ab initio* potential is referred to as potential A. The difference potential $V_2(R,\theta)$ was expanded as in Eq. (24), with $f(\theta)=C_2^2(\theta,0)$ and with $[C_6]_{22}$ calculated by scaling the *ab initio* value of $V_{22}(R)$ at $R=14a_0$. The spectroscopic observables calculated for potential A are listed in Table II. The stretching frequencies and rotational constants are clearly underestimated, the pattern of bending states for $n=0$ is only qualitatively correct, and the parity splittings are very far from their experimental measurements. We thus require an increase in ϵ_{00}^{Π}, decrease in $[R_m^{\Pi}]_{00}$ and a readjustment of the parameters determining the anisotropy.

As a first step in fitting, we determined a potential that reproduces the bending frequencies for $n=0$, the stretching frequencies for $\Delta n=1$, 2, and 3 and the parity doubling $\Delta\nu_{1/2}$; in addition, we constrained the potential to agree with the *ab initio* coefficient $V_{22}(R)$ at short range ($R=4a_0$), so that the strength of the difference potential at short range is reproduced. This set of observables [including the constraint on $V_{22}(R)$, which was actually included as a data point] will be referred to below as set $E1$. This fit was achieved by varying ϵ_{10}^{Π}, ϵ_{20}^{Π}, ϵ_{30}^{Π}, $v^{(2)}$, and $\beta^{(2)}$ in addition to ϵ_{00}^{Π} and $[R_m^{\Pi}]_{00}$, and constraining the remaining parameters to their *ab initio* values. However, the resulting potential gives bending frequencies for $n\geqslant 1$ that are too high by up to 2 or 3 cm^{-1}, and thus evidently has an incorrect R dependence of the anisotropic coefficients.

The radial dependence of the anisotropy might in principle be improved by modifying any of $[R_m^{\Pi}]_{10}$, $[R_m^{\Pi}]_{20}$, β_{10}^{Π}, or β_{20}^{Π}. However, for $n\geqslant 1$, the $P=-\frac{1}{2}$ and $P=-\frac{3}{2}$ states are close together and have not been resolved. Thus the only bending frequency that is known accurately for $n=1$, 2, and 3 is the separation between the $P=+\frac{3}{2}$ and $P=+\frac{1}{2}$ states. In first order, these separations are proportional to the *sum* of expectation values of $\langle V_{10}\rangle+\langle V_{20}\rangle$ for the stretching state concerned. Neither of the bending states is sensitive to the behavior of the potential for $\theta>90°$, so we applied the constraints $R_m^{\Pi}(180°)-R_m^{\Pi}(90°)=C_R$ and $\beta^{\Pi}(180°)-\beta^{\Pi}(90°)=C_\beta$, where C_R and C_β are *ab initio* values. To achieve this, $[R_m^{\Pi}]_{30}$, $[R_m^{\Pi}]_{40}$, β_{30}^{Π}, and β_{40}^{Π} were constrained to their *ab initio* values, and $[R_m^{\Pi}]_{10}$ and β_{10}^{Π} were constrained according to $[R_m^{\Pi}]_{10}=\frac{3}{2}[R_m^{\Pi}]_{20}-[R_m^{\Pi}]_{30}+\frac{5}{8}[R_m^{\Pi}]_{40}+C_R$ and $\beta_{10}^{\Pi}=\frac{3}{2}\beta_{20}^{\Pi}-\beta_{30}^{\Pi}+\frac{5}{8}\beta_{40}^{\Pi}+C_\beta$.

The enlarged data set $E2$, formed from set $E1$ and the first bending frequency for each of $n=1$, 2, and 3, allows only one extra parameter to be floated because of the high correlations between parameters. Set $E2$ can be fitted satisfactorily by floating $[\beta^{\Pi}]_{20}$ or $[R_m^{\Pi}]_{20}$ with the constraint described above. However, when $[R_m^{\Pi}]_{20}$ is floated, the quality of the fit is poorer than for $[\beta^{\Pi}]_{20}$ and the resulting coefficients $V_{10}(R)$ and $V_{20}(R)$ have a short range behavior qualitatively in disagreement with the *ab initio* potential. A more satisfactory fit is obtained by floating $[\beta^{\Pi}]_{20}$ in addition to parameter set $P1$. This enlarged parameter set is referred to as set $P2$; the optimized values and 95% confidence limits of the parameters are given in Table III and the correlation matrix is given in Table IV.

Contour plots of the resulting potential energy surfaces $V_{\Pi}(R,\theta)$ and $V_2(R,\theta)$ are shown in Fig. 1, and the potential coefficients $V_{lm}(R)$ are shown in Fig. 2. As expected, the potential is substantially deeper than the *ab initio* prediction at all geometries. The fitted potential V_{Π} is very flat as a function of θ near $\theta=0$, and varies by only 0.5 cm^{-1} between $\theta=0$ and 30°: The minimum in the fitted potential is actually nonlinear, near $\theta=15°$, but this feature

TABLE III. Comparison between the optimized values of the potential parameters (with their 95% confidence limits) and the parameters based on the *ab initio* potential.

	Potential A	Best fit	95% confidence limit
V_Π potential			
ϵ_{00}^Π (cm^{-1})	68.996	100.894	4.10
ϵ_{10}^Π (cm^{-1})	15.533	22.226	0.25
ϵ_{20}^Π (cm^{-1})	16.732	14.752	0.67
ϵ_{30}^Π (cm^{-1})	2.389	−12.456	2.08
ϵ_{40}^Π (cm^{-1})	0.454	0.454	*ab initio* value
$[R_m^\Pi]_{00}$ (a_0)	7.002 5	6.657 4	0.02
$[R_m^\Pi]_{10}$ (a_0)	0.080 08	0.080 08	*ab initio* value
$[R_m^\Pi]_{20}$ (a_0)	0.082 29	0.082 29	*ab initio* value
$[R_m^\Pi]_{30}$ (a_0)	0.098 68	0.098 68	*ab initio* value
$[R_m^\Pi]_{40}$ (a_0)	0.010 14	0.010 14	*ab initio* value
β_{00}^Π (a_0^{-1})	1.827 65	1.780 00	0.13
β_{10}^Π (a_0^{-1})	−0.030 317 6	0.211 39	constrained
β_{20}^Π (a_0^{-1})	0.041 934 2	0.203 10	0.003
β_{30}^Π (a_0^{-1})	0.012 607 6	0.012 607 6	*ab initio* value
β_{40}^Π (a_0^{-1})	0.021 513 1	0.021 513 1	*ab initio* value
V_2 potential			
$v^{(2)}$ (cm^{-1})	56.764	15.613	1.77
$\beta^{(2)}$ (a_0^{-1})	1.686 0	2.169 9	0.04
$[C_6]_{22}$ ($E_h a_0^6$)	3.425 4	3.425 4	*ab initio* value

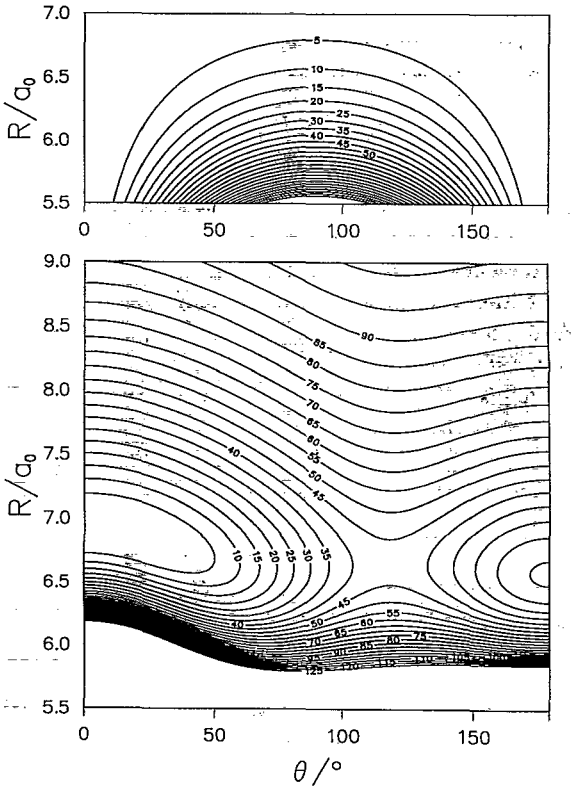

FIG. 1. Contour plots of the fitted potentials $V_\Pi(R,\theta)$ (lower panel) and $V_2(R,\theta)$ (upper panel) for Ar–OH ($X\,^2\Pi$). Contours for $V_\Pi(R,\theta)$ are drawn relative to the potential minimum at −125.93 cm^{-1}. Contour labels are in cm^{-1}.

is not reliably determined by the existing data. The barrier to internal rotation between the two minima at $\theta \approx 0$ and $\theta = 180°$ is 43.6 cm^{-1}, which is actually smaller than for the *ab initio* potential. The experimental data have determined the change in the repulsive wall anisotropy between linear and perpendicular geometries along the line in parameter space given by the constraint on β_{10}^Π above. The resolution of the $P=-\frac{1}{2}$ and $P=-\frac{3}{2}$ states for $n \geqslant 1$ should allow the separate determination of β_{10}^Π and β_{20}^Π. Unfortunately, the existing experimental data are not accurate enough to determine the angle dependence of the position of the minimum $R_m^\Pi(\theta)$. For this, high-precision rotational constants for the $P=+\frac{1}{2}$, $P=-\frac{1}{2}$, and $P=-\frac{3}{2}$ bending levels would be required.

It may be noted that the experimental observables fitted so far do not include the ground-state parity doubling $\Delta\nu_{3/2}$, which Ohshima, Iida, and Endo[16] have obtained from their microwave spectra. As has been discussed before,[21] simple models of the parity splittings make it difficult to reconcile the experimental value of $\Delta\nu_{3/2}$ with the bending frequencies and $\Delta\nu_{1/2}$ values from the SEP spectra. In the present work, we have devoted considerable effort to finding a potential that can resolve the discrepancy.

As described in Refs. 20 and 21, the parity doublings in both $P=+\frac{1}{2}$ and $P=+\frac{3}{2}$ states arise from matrix elements of $V_2(R,\theta)$ that connect the $\omega=\frac{3}{2}$ and $\omega=\frac{1}{2}$ manifolds. If only the V_{22} contribution to $V_2(R,\theta)$ is considered, and van der Waals stretching motions are neglected, the models of Refs. 20 and 21 yield Eqs. (26) and (27) above. The *ratio* of $\Delta\nu_{1/2}$ and $\Delta\nu_{3/2}$ thus largely depends only on the rotational constants and on the pattern of energy levels. Even though this conclusion was originally obtained on the basis of a simplified treatment, we show below that it appears to hold quite well for accurate calculations on real-

TABLE IV. Correlation matrix of fitted parameters.

	ϵ_{00}^Π	ϵ_{10}^Π	ϵ_{20}^Π	ϵ_{30}^Π	$[R_m^\Pi]_{00}$	β_{00}^Π	β_{20}^Π	$v^{(2)}$	$\beta^{(2)}$
ϵ_{00}^Π	1.000								
ϵ_{10}^Π	−0.134	1.000							
ϵ_{20}^Π	0.066	−0.220	1.000						
ϵ_{30}^Π	0.062	−0.459	−0.454	1.000					
$[R_m^\Pi]_{00}$	0.296	−0.082	0.092	0.063	1.000				
β_{00}^Π	−0.968	0.133	−0.084	−0.076	−0.311	1.000			
β_{20}^Π	−0.704	−0.056	0.065	0.021	0.209	−0.670	1.000		
$v^{(2)}$	−0.068	0.057	0.336	0.013	0.434	0.063	−0.005	1.000	
$\beta^{(2)}$	0.067	−0.056	−0.331	−0.013	−0.428	−0.063	0.005	−0.989	1.000

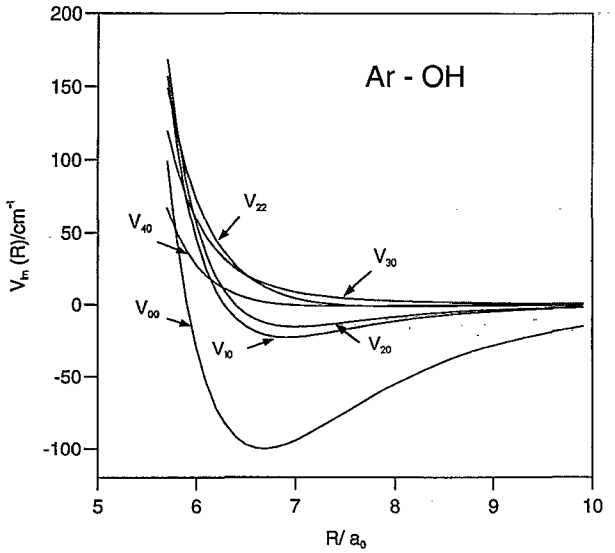

FIG. 2. Coefficients of the fitted potentials for Ar–OH ($X^2\Pi$) in a spherical harmonic expansion [Eqs. (9) and (10)].

istic potentials. Unfortunately, the ratio $\Delta\nu_{3/2}/\Delta\nu_{1/2}$ calculated from the fitted potential above for $J=\frac{3}{2}$ (3.17×10^{-4}) is quite different from the experimental ratio (7.33×10^{-4}).

There are various possible explanations for this effect, which we will consider in turn. First, it is possible that the true functional form of $V_2(R,\theta)$ is poorly represented by Eq. (24) with $f(\theta)=C_2^2(\theta,0)$. The angular wave function for $P=+\frac{3}{2}$ samples angles nearer $\theta=0$ than that for $P=+\frac{1}{2}$, so that the large experimental value of $\Delta\nu_{3/2}$ suggests an angular form of $f(\theta)$ which peaks at small values of θ. In order to investigate whether a different angular function could have the desired effect, we introduced a $V_2(R,\theta)$ anisotropy with

$$f(\theta)=\sin^2[\pi(\theta/\pi)^{\exp x}]. \tag{28}$$

This $f(\theta)$ is a function that is zero at $\theta=0$ and $\theta=180°$, but has a maximum at an intermediate angle which can be varied by changing x. The use of $\exp x$ rather than x itself ensures that the exponent cannot be negative. For fixed values of x, fits to the experimental set $E2$ were performed. However, we found that the calculated value of $\Delta\nu_{3/2}$ did not change by more than 4%, even for x as large as -1.6. We thus conclude that we cannot fit $\Delta\nu_{3/2}$ and $\Delta\nu_{1/2}$ simultaneously by altering the angular form of $V_2(R,\theta)$.

Another possible explanation for the discrepancy is that the neglect of the van der Waals stretching motion is important. This could arise either because the $P=+\frac{1}{2}$ and $P=+\frac{3}{2}$ states sample different ranges of the intermolecular distance R, or because matrix elements (of either V_Π or V_2) off-diagonal in the van der Waals stretching quantum number n (which were neglected in Refs. 20 and 21) are important. The former explanation seems rather unlikely, because the rotational constants for the $P=+\frac{1}{2}$ and $P=+\frac{3}{2}$ states are so similar.

In order to investigate the effects of the R dependence of V_Π, we investigated whether changes in $[R_m^\Pi]_{10}$ and $[R_m^\Pi]_{20}$ have any significant effect on the ratio $\Delta\nu_{3/2}/\Delta\nu_{1/2}$. We carried out fits to an enlarged observable set, formed from the set $E2$ and the parity doubling $\Delta\nu_{3/2}$, by floating an enlarged set of parameters formed from parameter set $P2$ and either $[R_m^\Pi]_{10}$ or $[R_m^\Pi]_{20}$. Although the parameters changed significantly, $[R_m^\Pi]_{10}=-0.273a_0$ and $[R_m^\Pi]_{20}=0.245a_0$, the ratio $\Delta\nu_{3/2}/\Delta\nu_{1/2}$ improved by only about 5%.

It is also possible that off-diagonal matrix elements of $V_2(R,\theta)$ itself are important. We carried out fits to the observable set $E2$, with the parameter set $P2$, for various reasonable values of $[C_6]_{22}$. For $[C_6]_{22}$ ranging from 0 to $6E_h a_0^6$, the ratio of the parity splittings improved by only about 1%, ruling out the importance of these off-diagonal matrix elements.

The discrepancy between the calculated and experimental values of $\Delta\nu_{3/2}$ thus remains unresolved. Despite extensive efforts, we have been unable to find a physically acceptable potential that can reproduce the experimental ratio $\Delta\nu_{3/2}/\Delta\nu_{1/2}$. If we could introduce a P-independent matrix element that couples different ω states in the same way as the V_{22} interaction, or in the same way as the monomer λ-doubling interaction, then we could reproduce the experimental ratio. Unfortunately, we have not found any physical justification for such a term. It would be very valuable to have experimental information on the parity doublings in additional states to help resolve the problem. In order to get information on $V_{32}(R)$ and higher terms, we would need experimental values for the parity doublings of the bending levels $P=-\frac{1}{2}$ and $P=-\frac{3}{2}$, which sample angles $\theta\geqslant90°$. Similarly, parity doublings for excited stretching states would allow us to determine the R dependence of $V_2(R,\theta)$.

V. PREDICTIONS

We have used our fitted potential to calculate the energies and rotational constants of a large number of excited states. These predictions may help in assigning additional bands in the SEP spectrum, and also provide predictions that may be useful in future studies of the far-infrared or mid-infrared spectrum.

We have carried out close-coupling calculations on all the states correlating with $j=\frac{3}{2}$, $\omega=\frac{3}{2}$ for $n\leqslant4$, and the results are given in Table V. Some of the frequencies given are of course among those fitted in obtaining the potential. The results confirm that the $P=-\frac{3}{2}$ and $-\frac{1}{2}$ states are within 1.5 cm^{-1} of one another for $n>0$. It may be noted that the levels for $n=4$ are bound for our fitted potential, though Berry *et al.*[15] believed them to be unbound on the basis of a Birge–Sponer extrapolation.

At higher energies, the density of states is larger and it becomes increasingly difficult to assign unambiguous quantum numbers to results from close-coupling calculations. Accordingly, we have characterized the states correlating with $j>\frac{3}{2}$ or $\omega=\frac{1}{2}$ using helicity decoupling calculations in a body-fixed basis set, neglecting all Coriolis matrix off-diagonal in P. Since calculations are performed for each value of $|P|$ separately, the assignment problem is simplified. Additional information on the character of each state

TABLE V. Spectroscopic properties of Ar–OH ($X^2\Pi$) from close-coupling calculations on the fitted potential. The energies are given for $J=\frac{3}{2}$ and correspond to the average of the two parity components. Stretching frequencies are given relative to the ground state, and bending frequencies relative to the lowest bending state of the same manifold. All quantities are in cm^{-1}, and numbers in parentheses indicate powers of 10.

n	P	Energy	Bend	Stretch	B_P^n	$\Delta\nu_P$ $(J=\frac{3}{2})$
0	+3/2	−95.499			0.1025	7.29(−5)
0	+1/2	−85.804	9.695		0.1076	0.230
0	−1/2	−76.300	19.199		0.0985	−0.209
0	−3/2	−74.199	21.300		0.1259	−3.81(−3)
1	+3/2	−60.622		34.877	0.0924	1.25(−4)
1	+1/2	−54.226	6.396		0.0975	0.257
1	−1/2	−47.697	12.925		0.0860	−0.233
1	−3/2	−46.245	14.377		0.1161	−7.14(−3)
2	+3/2	−34.936		60.563	0.0809	2.52(−4)
2	+1/2	−30.848	4.088		0.0858	0.266
2	−1/2	−26.441	8.495		0.0724	−0.233
2	−3/2	−25.458	9.478		0.1036	−1.19(−2)
3	+3/2	−17.430		78.069	0.0675	5.61(−4)
3	+1/2	−14.853	2.577		0.0722	0.249
3	−1/2	−12.055	5.375		0.0563	−0.200
3	−3/2	−11.454	5.976		0.0882	−2.04(−1)
4	+3/2	−6.945		88.554	0.0566	4.21(−3)
4	+1/2	−5.404	1.541		0.0562	0.226
4	−1/2	−3.834	3.111		0.0380	−0.172
4	−3/2	−3.521	3.424		0.0680	−7.98(−2)

may be obtained by examining the eigenvector corresponding to the smallest eigenvalue of the log-derivative matching matrix, which may be shown to be proportional to the wave function at the matching point R_{mid}.

A further problem for states above the dissociation threshold is that they can predissociate, and should really be characterized by performing scattering calculations and analyzing the resonances that occur.[35] However, since the states are predominantly bound in character, it is a reasonable approximation to apply bound-state boundary conditions and neglect the continuum part of the wave functions (while still including the "open" channels in the calculations). This can be done with the BOUND program; in addition to the real quasibound states, it gives spurious eigenvalues corresponding to box-quantized continuum states in the open channels. However, these spurious eigenvalues are readily identified because their energies are strongly dependent on the outer propagation limit R_{max}.

The states correlating with $\omega=\frac{1}{2}$ and $\omega=\frac{3}{2}$, $j>\frac{3}{2}$ are listed in Table VI. We estimate that the helicity decoupling approximation is accurate to ± 0.2 cm^{-1} in the worst cases, and that the approximate treatment of the continuum causes shifts of up to 0.1 cm^{-1}. Quantum number assignments have been given for most levels, though there is one pair that is too strongly mixed for this to be reliable; this is indicated in the table. The pattern of energy levels is shown in Fig. 3.

For $\omega=\frac{3}{2}$, $j=\frac{5}{2}$, the lowest bending level ($P=+\frac{5}{2}$) is below the dissociation limit for OH ($X^2\Pi$, $n=0$, $j=\frac{3}{2}$) for this potential, and is truly bound. All the remaining bend-

TABLE VI. Calculated energy levels for Ar–OH ($X^2\Pi$) from helicity decoupling calculations on the fitted potential. All calculations are for $J=P$, and are given in cm^{-1} relative to the ground state at -95.50 cm^{-1}. Quantum numbers have been assigned where possible. The sign of P (relative to ω) is given where it is clear from our calculations; where the sign is not given, it has not been unambiguously determined.

j	ω	n	P	Energy
5/2	3/2	0	+5/2	88.07
5/2	3/2	0	+1/2	95.75
5/2	3/2	0	+3/2	95.82
5/2	3/2	0	−1/2	98.84
5/2	3/2	0	−3/2	99.17
5/2	3/2	0	−5/2	107.12
5/2	3/2	1	+5/2	121.52
5/2	3/2	1	+1/2	125.60
5/2	3/2	1	+3/2	128.59
5/2	3/2	1	−3/2	130.48
5/2	3/2	1	−1/2	130.62
5/2	3/2	1	−5/2	134.33
1/2	1/2	0	+1/2	132.70
1/2	1/2	0	−1/2	145.55
5/2	3/2	2	+5/2	146.39
5/2	3/2	2	+1/2	149.37
5/2	3/2	2	+3/2	150.10
5/2	3/2	2	−3/2	150.87
5/2	3/2	2	−1/2	151.47
5/2	3/2	2	−5/2	154.62
5/2	3/2	3	+5/2	163.45
5/2	3/2	3	+1/2	164.07
5/2	3/2	3	+3/2	166.10
5/2	3/2	3	−1/2	166.84[a]
1/2	1/2	1	+1/2	167.37[a]
5/2	3/2	3	−3/2	167.87
5/2	3/2	3	−5/2	168.27
5/2	3/2	4	3/2	173.42
5/2	3/2	4	−5/2	173.72
5/2	3/2	4	+1/2	174.79
5/2	3/2	4	3/2	174.90
1/2	1/2	1	−1/2	175.37
5/2	3/2	4	+5/2	175.72
1/2	1/2	2	+1/2	190.33
1/2	1/2	2	−1/2	195.30
3/2	1/2	0	+3/2	198.25
3/2	1/2	0	+1/2	198.37
3/2	1/2	0	−1/2	201.97
1/2	1/2	3	+1/2	208.12
3/2	1/2	0	−3/2	208.90
7/2	3/2	0	+7/2	209.02
1/2	1/2	3	−1/2	210.88
7/2	3/2	0	1/2	214.10
7/2	3/2	0	3/2	215.13
7/2	3/2	0	5/2	215.34
1/2	1/2	4	+1/2	216.73
7/2	3/2	0	3/2	218.22
7/2	3/2	0	5/2	218.41
7/2	3/2	0	1/2	218.56
7/2	3/2	0	−7/2	225.92
3/2	1/2	1	1/2	230.16
3/2	1/2	1	3/2	230.20
3/2	1/2	1	1/2	232.15
3/2	1/2	1	3/2	238.28
7/2	3/2	1	+7/2	241.60
7/2	3/2	1	1/2	245.95
7/2	3/2	1	5/2	246.69
7/2	3/2	1	3/2	247.34
7/2	3/2	1	5/2	248.39
7/2	3/2	1	1/2	249.32
7/2	3/2	1	3/2	252.33
7/2	3/2	1	−7/2	253.04

[a]These two levels are strongly mixed, and the quantum number assignments are uncertain.

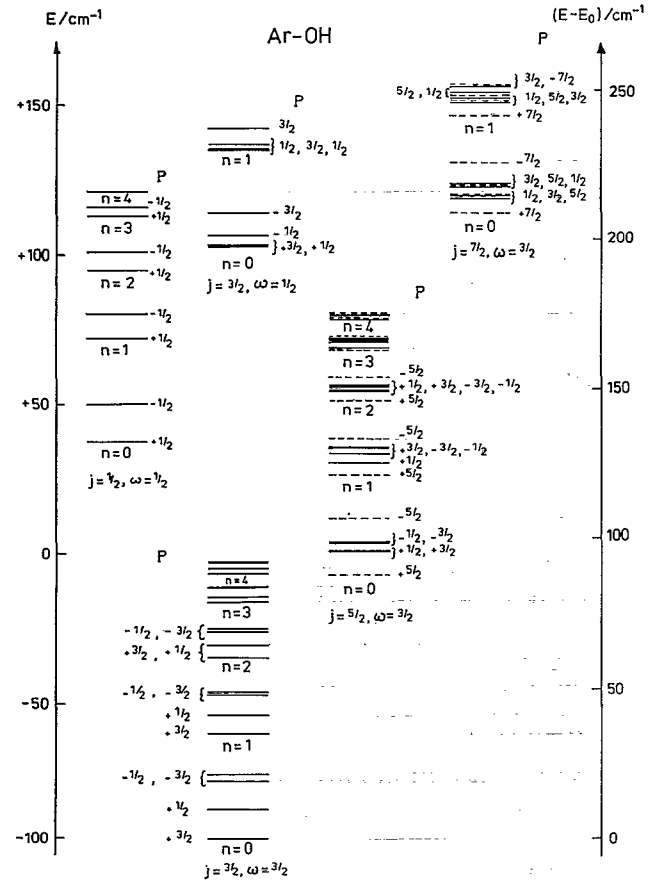

FIG. 3. Energy levels of Ar–OH ($X^2\Pi$) calculated using the fitted potential. Levels with $|P| > \frac{5}{2}$, which are expected to be forbidden in SEP spectra involving an excited state with no vibrational angular momentum, are shown as dashed lines.

ing states are quasibound, and will undergo rotational predissociation, converting OH internal rotational energy to relative translation of the fragments.

The SEP spectra of Berry *et al.*[15] were obtained by pumping electronically excited levels with no bending excitation and no vibrational angular momentum. In a closed-shell molecule, these states would undergo stimulated emission with the selection rule $\Delta K = 0, \pm 1$. This will be slightly relaxed in Ar–OH, since the electron spin can contribute $\pm\frac{1}{2}$ to P. However, ground-state levels with $|P| > \frac{3}{2}$ are still expected to be inaccessible from A state levels with no bending excitation, except for the effects of Coriolis coupling. In addition, because the excited-state levels have wave functions concentrated around $\theta = 0$, transitions to ground-state levels with $P > 0$ are expected to have more favorable Franck–Condon factors than those to levels with $P < 0$.

Berry *et al.*[15] observed peaks 89, 94, 97, and 103 cm^{-1} above the ground state which they attributed to $j = \frac{5}{2}$, $\omega = \frac{3}{2}$, $n = 0$. Although our calculations do give the $P = +\frac{5}{2}$ state at 88.07 cm^{-1}, we expect transitions to this to be forbidden in the SEP spectrum. It seems more likely that the peak at 89 cm^{-1} is due to the $j = \frac{3}{2}$, $P = +\frac{3}{2}$, $n = 4$ state which is predicted at 88.5 cm^{-1}. The peaks at 94 and 97 cm^{-1} agree reasonably well with our predicted $|P| = \frac{1}{2}$ and $\frac{3}{2}$ states at 95.7, 95.8, 98.8, and 99.1 cm^{-1}. However, this leaves the peak at 103 cm^{-1} unassigned, since transitions to the $P = -\frac{5}{2}$ state (predicted at 107.1 cm^{-1}) are again expected to be forbidden. It does appear from the SEP spectrum (Fig. 6 of Ref. 15) that each $j = \frac{5}{2}$ manifold, for $n = 0$, 1, and 2, has a sharp peak 4–6 cm^{-1} above the main broad feature. Our potential does not predict this, though the broad features for $n = 1$, 2, and 3 at 125, 149, and 166 cm^{-1} are reasonably well reproduced in our calculations by groups of levels at 126–130, 148–151, and 164–167 cm^{-1}. However, it may be noted that the $j = \frac{5}{2}$ levels are sensitive to higher-order Legendre contributions to the potential ($l = 4$ and 5) which have no diagonal matrix elements for $j = \frac{3}{2}$ and thus little effect on the $j = \frac{3}{2}$ level structure. If the $j = \frac{5}{2}$ levels can be conclusively assigned, they may allow these higher-order anisotropies to be determined.

The bound states for $j = \frac{7}{2}$ start 209 cm^{-1} above the ground state for our potential. However, as for $j = \frac{5}{2}$, the only allowed transitions in the SEP spectra will be to states with $|P| = \frac{1}{2}$ and $\frac{3}{2}$, which are predicted between 214 and 219 cm^{-1}. Berry *et al.*[15] assigned a large broad feature between 208 and 214 cm^{-1} to the $j = \frac{7}{2}$ states. This assignment is plausible, though there are also some $\omega = \frac{1}{2}$ states in this region.

The $\omega = \frac{1}{2}$ states present an assignment problem, as discussed by Berry *et al.*[15] The very strong peak observed at 139 cm^{-1} must be one of the two components of the $j = \frac{1}{2}$, $\omega = \frac{1}{2}$ manifold, with $P = \pm\frac{1}{2}$. However, our fitted potential gives a splitting of 12.86 cm^{-1} between the two components, with the $P = +\frac{1}{2}$ component, expected to be the more intense, at 132.6 cm^{-1}. It is possible that the monomer spin–orbit coupling constant is modified in the complex, and this would shift all the $\omega = \frac{1}{2}$ levels up or down with respect to the $\omega = \frac{3}{2}$ levels. We attempted to fit a new potential with a modified spin–orbit coupling constant, on the assumption that the peak at 139 cm^{-1} peak is due to the $\omega = \frac{1}{2}$, $P = +\frac{1}{2}$ state, and found that the energy level pattern was indeed almost unchanged apart from a global shift of the $\omega = \frac{1}{2}$ levels. However, there is no peak in the SEP spectrum near 152 cm^{-1} that might be assigned to the $P = -\frac{1}{2}$ component. There seem to be three possibilities.

(i) The $P = -\frac{1}{2}$ component has very little intensity, and is unobserved.

(ii) The $P = -\frac{1}{2}$ peak is hidden underneath the broad feature at 149 cm^{-1}. This would imply that the separation of the two components is overestimated by about 2 cm^{-1}.

(iii) The $P = -\frac{1}{2}$ component is responsible for the peak at 154 cm^{-1}. This is in some ways the most attractive possibility, since the 154 cm^{-1} peak is not satisfactorily assigned as a component of $j = \frac{5}{2}$ by our potential. However, it would leave us without assignments for the peaks at 103 and 131 cm^{-1}, which were also tentatively attributed to $j = \frac{5}{2}$ above. Thus there is no entirely satisfactory identification of the $\omega = \frac{1}{2}$ peaks, and further experimental work is needed.

Berry *et al.*[15] have commented that the relative intensities of different bands in the SEP spectrum are different when different vibrational levels of the A state are pumped. In particular, they observed stronger excitation of bending

levels when the $n'=5$ level was pumped, and attributed this to contamination of this excited state by excited bending levels. Such an effect will indeed improve the Franck–Condon factors for transitions to excited stretching levels, but will not in itself relax the angular momentum constraint that restricts the levels populated to $|P| \leqslant \frac{3}{2}$. It would be particularly interesting to carry out SEP experiments dumping from electronically excited states with vibrational angular momentum, since this would make additional bending states, with $|P| > \frac{3}{2}$, accessible.

VI. CONCLUSIONS

We have obtained an empirical potential for the interaction of OH ($X^2\Pi$) with Ar, by fitting to energy levels obtained from stimulated-emission pumping (SEP)[14,15] and microwave[16] spectra. The potential accurately reproduces all the van der Waals bending and stretching levels correlating with OH in its $\omega=\frac{3}{2}$, $j=\frac{3}{2}$ state. However, despite considerable effort, we have been unable to find a potential that is simultaneously capable of reproducing both the ground-state ($P=+\frac{3}{2}$) parity doubling constant of Ohshima, Iida, and Endo[16] and the excited-state ($P=+\frac{1}{2}$) parity doubling constant of Berry *et al.*[14]

We have used the fitted potential to calculate a large number of van der Waals excited states of OH ($X^2\Pi$) and have compared the results with the SEP spectra. The agreement is in general fairly good, though there are some points of difficulty. We suggest that it would be very valuable to observe SEP spectra dumping from an electronically excited state with vibrational angular momentum, since this should allow additional bending states to be observed.

ACKNOWLEDGMENTS

The authors are grateful to Dr. David Flower for helpful discussions. This work is supported by the Science and Engineering Research Council.

[1] For a review of this work, see M. C. Heaven, Ann. Rev. Phys. Chem. **43**, 283 (1992).
[2] W. M. Fawzy and M. C. Heaven, J. Chem. Phys. **89**, 7030 (1988).
[3] W. M. Fawzy and M. C. Heaven, J. Chem. Phys. **92**, 909 (1990).
[4] M. T. Berry, M. R. Brustein, J. R. Adamo, and M. I. Lester, J. Phys. Chem. **92**, 5551 (1988).
[5] M. T. Berry, M. R. Brustein, and M. I. Lester, Chem. Phys. Lett. **153**, 17 (1988).
[6] M. T. Berry, M. R. Brustein, and M. I. Lester, J. Chem. Phys. **90**, 5878 (1989).
[7] K. M. Beck, M. T. Berry, M. R. Brustein, and M. I. Lester, Chem. Phys. Lett. **162**, 203 (1989).
[8] M. T. Berry, M. R. Brustein, and M. I. Lester, J. Chem. Phys. **92**, 6469 (1990).
[9] J. M. Bowman, B. Gadzy, P. Schafer, and M. C. Heaven, J. Phys. Chem. **94**, 2226 (1990).
[10] U. Schnupf, J. M. Bowman, and M. C. Heaven, Chem. Phys. Lett. **189**, 487 (1992).
[11] J. Schleipen, L. Nemes, J. Heinze, and J. J. ter Meulen, Chem. Phys. Lett. **175**, 561 (1990).
[12] B.-C. Chang, L. Yu, D. Cullin, B. Rehfuss, J. Williamson, T. A. Miller, W. M. Fawzy, X. Zheng, S. Fei, and M. Heaven, J. Chem. Phys. **95**, 7086 (1991).
[13] M. I. Lester, R. A. Loomis, L. C. Giancarlo, M. T. Berry, C. Chakravarty, and D. C. Clary, J. Chem. Phys. **98**, 9320 (1993).
[14] M. T. Berry, M. R. Brustein, M. I. Lester, C. Chakravarty, and D. C. Clary, Chem. Phys. Lett. **178**, 301 (1991).
[15] M. T. Berry, R. A. Loomis, L. C. Giancarlo, and M. I. Lester, J. Chem. Phys. **96**, 7890 (1992).
[16] Y. Ohshima, M. Iida, and Y. Endo, J. Chem. Phys. **95**, 7001 (1991).
[17] A. Degli Esposti and H.-J. Werner, J. Chem. Phys. **93**, 3351 (1990).
[18] C. Chakravarty, D. C. Clary, A. Degli Esposti, and H.-J. Werner, J. Chem. Phys. **93**, 3367 (1990).
[19] M.-L. Dubernet, D. R. Flower, and J. M. Hutson, J. Chem. Phys. **94**, 7602 (1991).
[20] W. H. Green and M. I. Lester, J. Chem. Phys. **96**, 2573 (1992).
[21] M.-L. Dubernet, P. A. Tuckey, and J. M. Hutson, Chem. Phys. Lett. **193**, 355 (1992).
[22] J. M. Hutson, Ann. Rev. Phys. Chem. **41**, 123 (1990).
[23] J. M. Brown, M. Kaise, C. M. L. Kerr, and D. J. Milton, Mol. Phys. **36**, 553 (1978).
[24] J. A. Coxon, Can. J. Phys. **58**, 933 (1980).
[25] J. M. Hutson, Adv. Mol. Vib. Collision Dynam. **1A**, 1 (1991).
[26] H. Klar, J. Phys. B **6**, 2139 (1973).
[27] M. H. Alexander, J. Chem. Phys. **76**, 5974 (1982).
[28] B. R. Johnson, J. Chem. Phys. **69**, 4678 (1978).
[29] J. M. Hutson, BOUND computer code, version 3 (1986), distributed by Collaborative Computational Project No. 6 of the Science and Engineering Research Council (UK).
[30] J. M. Hutson, J. Chem. Phys. **96**, 6752 (1992).
[31] A. D. Buckingham, Adv. Chem. Phys. **12**, 107 (1967).
[32] K. T. Tang, Phys. Rev. **177**, 108 (1969).
[33] K. T. Tang and J. P. Toennies, J. Chem. Phys. **80**, 3726 (1984).
[34] W.-K. Liu, J. E. Grabenstetter, R. J. Le Roy, and F. R. McCourt, J. Chem. Phys. **68**, 5028 (1978).
[35] C. J. Ashton, M. S. Child, and J. M. Hutson, J. Chem. Phys. **78**, 4025 (1982).